Hindawi
Shock and Vibration
Volume 2020, Article ID 2749540, 10 pages
https://doi.org/10.1155/2020/2749540

Research Article

Experimental Investigation of Damage Evolution Characteristics of C50 Concrete under Impact Load

Mingfeng Lei,[1,2] Linghui Liu,[1] Yuexiang Lin,[3] Jianjun Ma,[4] Chenghua Shi,[1] and Weichao Yang[1]

[1]*School of Civil Engineering, Central South University, Changsha, China*
[2]*Key Laboratory of Engineering Structure of Heavy Haul Railway (Central South University), Changsha, China*
[3]*School of Aeronautics and Astronautics, Sun Yat-Sen University, Guangzhou 510006, China*
[4]*School of Civil Engineering, Sun Yat-Sen University, Guangzhou 510006, China*

Correspondence should be addressed to Yuexiang Lin; csulyx2010@csu.edu.cn

Received 25 October 2019; Revised 28 July 2020; Accepted 5 August 2020; Published 2 September 2020

Academic Editor: Alvaro Cunha

Impact loads widely exist in practical engineering and often cause cumulative damage and cracks or even fracture failure of concrete structures with their repeated long-term action. This experimental research is conducted on the damage evolution characteristics of concrete under impact loads by regarding C50 nonreinforced concrete as the research object and using a self-developed drop-weight device with electromechanical impedance measurement technology. Results show the following. (1) Under low-energy impact, concrete damage has long continuous development process and remarkable cumulative effects. An apparently sudden break characteristic appears before failure. Under high-energy impact, concrete damage accumulates rapidly, and piezoceramic patch signals grow linearly. (2) The root mean square deviation (RMSD) of the concrete increases exponentially with impact times. Particularly, when the RMSD exceeds 0.075, the concrete damage process enters the rapid development stage and approaches the critical failure state. (3) Under the experimental conditions in this study, the relationship between the ultimate impact times (damage life) and impact heights of the concrete samples shows the development trend of the power function. The above results can provide reference for the research on service life prediction methods of concrete structures under impact loads.

1. Introduction

Impact loads widely exist in the construction and operation of civil engineering structures, such as the blasting load caused by drilling and blasting during tunnel construction and the dynamic load of running high-speed trains. Loads with long-term and repeated action will inevitably lead to cumulative damage, crack initiation, and even the fracture failure of concrete structures with significant brittle mechanical properties. For example, a joint investigation of the Chengdu–Chongqing and Sichuan–Guizhou railway tunnel diseases in southwest China, which was conducted by Chengdu Railway Bureau and Central South University in 2015, found that the length proportions of tunnel sections with basement crack diseases have reached 13% (2643/20429 m). The typical structural diseases of tunnel bottoms are shown in Figures 1(a) and 1(b). In 2017–2018, the Taiyuan Railway Bureau and Central South University jointly investigated the diseases of the Daqin heavy haul railway in China and found that basement crack diseases accounted for 1/3 of all the diseases among the 39 tunnels in the railway works section of the Daqin Line, and the occurrence rate of these basement diseases was accelerating with time. Similar cases occur in bridge engineering. Damage cracks occur in the beam body of several bridges along a line with a width of 0.1–0.5 mm. Photos of typical cracks are shown in Figure 1(c). These diseases will cause serious guideway irregularities in the vertical and horizontal directions, which will negatively influence the driving safety. Moreover, they will reduce the bearing capacity of structures and endanger the safety and stability of structural systems; additional damage occurs particularly under impact loads.

(a) (b) (c)

Figure 1: Typical structural diseases: (a) faulting crack in fill layer of tunnel bottom; (b) minor cracks in tunnel rail plates; (c) vertical crack in beam body.

Therefore, researching the damage characteristics of concrete structures under impact loads, further exploring the damage development laws, and revealing the damage evolution mechanism of concrete structures are significant in theoretical foundation research.

The damage development of concrete is a progressive cumulative process with difficulties in characterization and measurement. At the end of the 20th century, Sun et al. [1] and Ayres et al. [2, 3] applied the electromechanical impedance (EMI) technique successively to the damage detection of a composite truss structure and a steel truss bridge; these studies verified the feasibility and effectiveness of the technology in the performance measurement of civil engineering structures. EMI has the following advantages: (1) excellent sensitivity in minor structural damage measurement and (2) an analysis process with no comprehension requirement to the original structure model. This method provides an effective means of engineering structural damage measurement. Giurgiutiu et al. [4] used EMI technology to measure the fatigue damage of a structural welding joint; they proposed a function between the structural residual life and the damage criterion based on the Euclid norm. Soh et al. [5] conducted EMI measurement on the crack development of a reinforced concrete beam bridge; root mean square deviation (RMSD) was defined as the damage degree criterion, and the results verified the high sensitivity of EMI technology. Bhalla et al. [6] performed an impedance experiment under the action of seismic waves on beam-column joints and the beam bottom span of reinforced concrete frame structures with one or two layers; they also proposed a quantitative criterion of the complex damage with enormous information and effective damage evaluations. Tseng and Wang [7, 8] used the impedance method to investigate the degradation law of material properties when the concrete suffers from environmental violations, and the measuring results are comparatively analyzed with numerical simulation results; this work validated the effectiveness of the impedance method in concrete damage extension detection. Scholars at the Huazhong University of Science and Technology in China [9, 10] conducted EMI measurements on steel beams and steel frames, along with the nonreinforced and reinforced concrete, which showed that EMI technology has good sensitivity in the detection of concrete crack, bolts, and other forms of damage. The association between damage location and macroscopic mechanical physical quantity, including damage criteria and strength, has been extensively investigated, and a wealth of experimental research results and experience has been attained. The author's team [11–14] also used EMI technology to perform a large number of experiments on the fatigue damage of tunnel bottom structures and proposed a fatigue damage model for such structures under the dynamic impact load of running trains.

In general, EMI technology has been widely recognized for structural damage identification and monitoring and has become a common research method in this research field. However, existing studies show that prefabricated crack damage is mostly used in damage construction, and the application and analysis of the results are mainly about the comparison of state signals before and after damage. Few studies focused on the full-time damage signals development. Thus, on the basis of previous works, a full-time EMI experiment of concrete under impact loads is conducted on the C50 nonreinforced concrete in this study. The damage evolution characteristics of the concrete members under the impact loads are discussed by analyzing the experimental results.

2. Experimental Program

2.1. Sample Preparation. C50 concrete, which is a commonly used structural concrete (strength grade), is selected as the testing sample. The mixing proportions and material requirements of the concrete are shown in Table 1. The sizes of the samples are $150 \times 150 \times 150$ mm and $100 \times 100 \times 300$ mm. Among the samples, nine test blocks ($150 \times 150 \times 150$ mm) are used for concrete strength calibration, and six test blocks ($100 \times 100 \times 300$ mm) are used for an impact damage test. The concrete is dry-mixed by a forced action mixer for 30 seconds with a total mixing time of 2 minutes. A slump test is carried out after the mixing; the results show that the controlled slumps are within the range of 5 cm and 10 cm. Then, a standard plastic mold is injected for coagulation casting and vibrated on an automatic vibrator for 60 seconds. Subsequently, steam curing is applied according to the curing system shown in Table 2. After 24 hours, the mold is removed and raised with water. After 7 days, it is

Table 1: Mixing proportions and material category requirements of the tested concrete (C50).

Material	Categories	Requirements	Mixing proportion (kg)
Cement	P.O. 42.5		380
Fly ash	Class I	Fineness < 12%; loss of ignition < 5%; activity index > 70%	100
Fine aggregate	Medium-sized sand	Mud content < 1.0%; mud clod content < 1.0%; fineness modulus < 3.0; range of aggregate with diameter below 0.315 mm is from 25% to 30%; apparent density > 2500 kg/m^3; bulk density > 1350 kg/m^3; content below 0.315 mm has particle size ranging from 25% to 30%; apparent density > 2500 kg/m^3; bulk density > 1350 kg/m^3	692
Coarse aggregate	5–25 mm continuous grading	Mud content < 1.5%; mud clod content < 0.5%; needle tablet content < 5%; apparent density > 2500 kg/m^3, bulk density > 1350 kg/m^3	1128
Water	Water	Pure water	150
Water-reducing agent	Solid polycarboxylic	High-performance water-reducing agent	0.5

Table 2: Steam curing systems.

Static curing (h)	Heating rate (°C/h)	Holding time (h)	Constant temperature (°C)	Cooling rate (°C/h)
3	15	3	50	15

placed in a standard incubation room with constant temperature and humidity till the 28th day.

2.2. Uniaxial Compressive Test. Uniaxial compressive strength tests are conducted on five concrete blocks ($150 \times 150 \times 150$ mm) to accurately calibrate the sample strength grade. The typical test process is shown in Figures 2(a) and 2(b), showing the curves of axial stress σ with the varying micro axial strain $\mu\varepsilon$ under the axial compression test. The average compressive strength of the samples is 52.4 MPa and Poisson's ratio is 0.23, which meet the requirements of the concrete grade.

2.3. Impact Test. In the 1960s, Green designed a drop-weight impact experimental device and corresponding experimental method. This technique has been widely used due to its simplicity and economy. In the following decades, many scholars have upgraded the device in accordance with their own demands. Referring to the free drop-weight test method recommended by the American Concrete Association, this study presents a self-designed and homemade experimental equipment, as shown in Figure 3. The test device is mainly composed of three parts: an impact ball, a guide cylinder, and a flexible plate. The weight of the impact ball is 4 kg, and the guide cylinder is made of polymethyl methacrylate. Scale lines are drawn on the cylinder wall to control and adjust the drop-impact height of the heavy ball. Test components with different damage degrees can be obtained by adjusting the impact heights and impact times. To ensure an even downward transmission of the impact force, and avoid device bottom secondary bound under the drop ball impact, flexible bottom plate is set below the force transmitting steel plate with a rigid base. Three impact heights (energies) (20, 25, and 30 cm) are considered during the impact test.

2.4. Test Equipment for Impact Damage. Research shows that EMI technology has a high sensitivity in structural damage identification and monitoring. In this experiment, the high sensitive PZT-5 piezoceramic patches and PV80-A impedance analyzer are selected to monitor the damage condition of the concrete sample; the test principle is shown in Figure 4 [15, 16]. The piezoceramic patch is a round piece with a diameter of 15 mm and a thickness of 0.5 mm. Flanged electrodes and AB adhesive are separately adopted for easy bonding between the PZT patches and the samples. PZT is arranged in accordance with the local effect of the piezoceramic patches to comprehensively realize the damage state of the concrete samples, as shown in Figure 5. The sweep frequency interval of the PV80-A impedance analyzer is 1 kHz–1 MHz.

3. Analysis of Experimental Results

3.1. Conductance Signal. Figure 6 shows the conductance signal test results with different measuring points and various impact times at 20 cm impact height. Figure 7 shows the conductance signal test results of the sample at the initial state and at the impact point when visible cracks appear. This analysis indicates the following:

(1) Test curve distributions of the measuring points at sample ends are dense. The conductance signal change is small, whereas the variation at the impact point is significant. These findings indicate that the concrete damage at the direct use point is more severe than that in the adjacent area. However, the EMI measurement method cannot reflect the overall damage state of samples with typical local effects; these results are consistent with those in the literature [17]. That is, the ideal testing range of the piezoceramic patches for the concrete damage is within 30 cm.

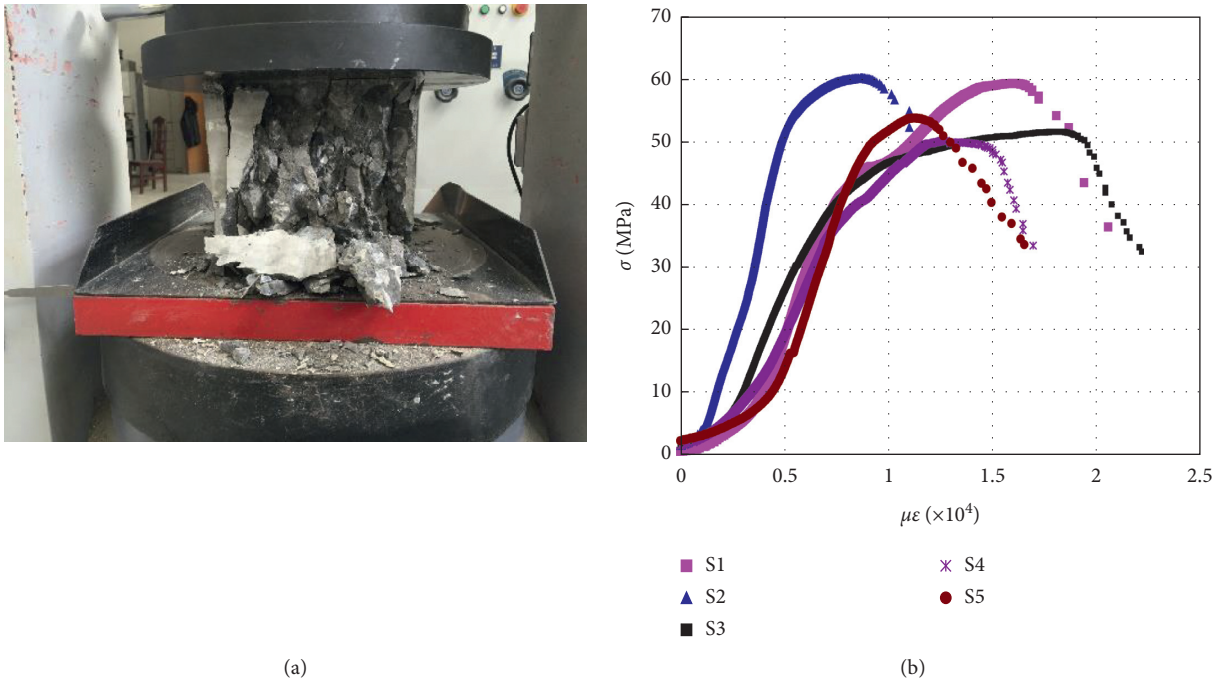

Figure 2: Uniaxial compressive strength test: (a) strength test of the cubic samples; (b) stress-strain curves.

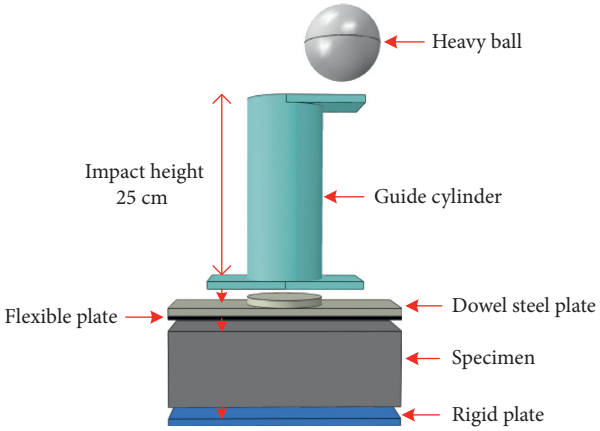

Figure 3: Drop-weight experiment equipment.

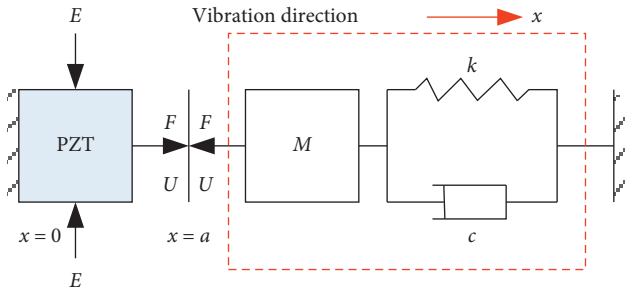

Figure 4: EMI measurement principle.

(2) In comparison with the initial state, the sample is impacted to the visible crack state, and the peak value of the conductance signal changes significantly with the remarkable deviation of the corresponding frequency. This result verifies the good discernibility of the piezoceramic patch signal to the mechanical characteristics of the concrete damage. Thus, the signal can be applied to study the damage evolution characteristics of the concrete.

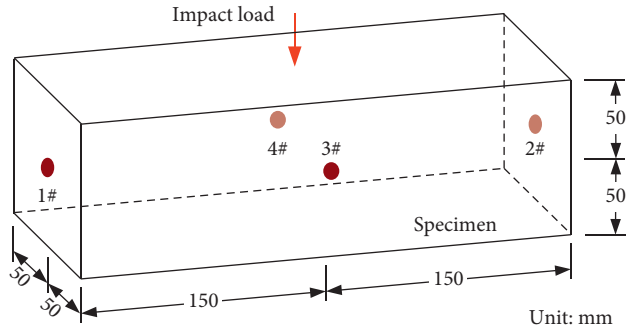

Figure 5: Location of piezoceramic patches.

(3) The conductance signal curves under various impact times are further analyzed. The conductance signal curves show the characteristic of continuous unidirectional changes with sudden break. Therefore, the change increment of the conductance signal is relatively small with limited impact times. However, when the continuous impact reaches sufficient times, the change increment of the conductance signal increases suddenly and considerably. This observation indicates that the concrete damage has a particular cumulative effect and a sudden break effect in terms of mechanical principles.

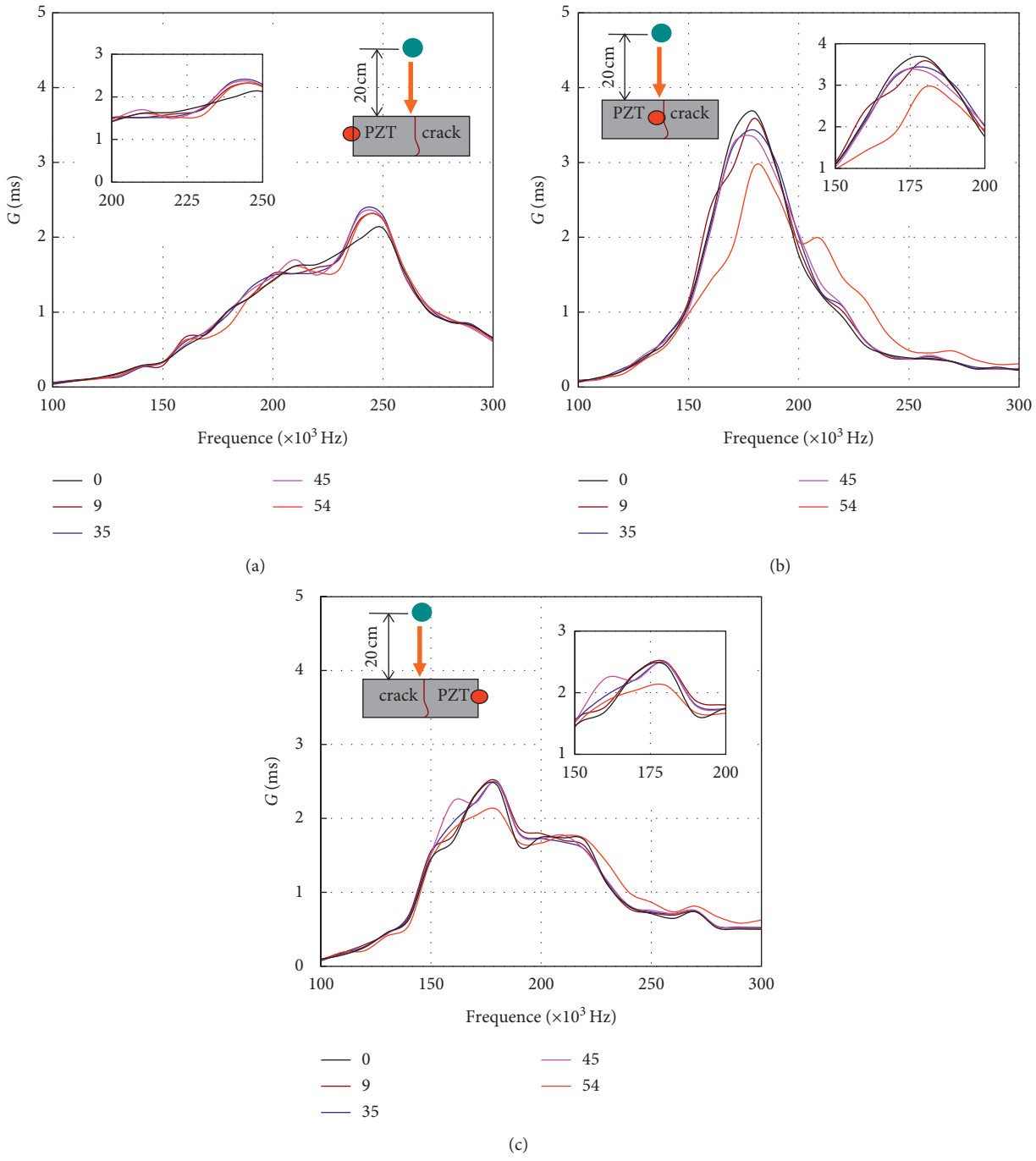

Figure 6: Conductance signal test results with 20 cm impact height: (a) −15 cm; (b) 0 cm; (c) 15 cm.

3.2. Law of Damage Evolution. The damage characteristics of the concrete under different impact times are qualitatively analyzed through the changes in the conductance signal distribution of the concrete samples. Although these test results can reflect the existence of concrete damage, the damage degree cannot be quantitatively characterized due to differences in the inherent characteristics of the piezoceramic patches used in the test. As shown in existing research results [9–11], the RMSD in the piezoceramic patch signal can well reflect the damage change of the test object, and the calculation formula is given as follows:

$$\mathrm{RMSD} = \sqrt{\frac{\sum_{i=1}^{N}\left(G_i^n - G_i^0\right)^2}{\sum_{i=1}^{N}\left(G_i^0\right)^2}}, \tag{1}$$

where G_i^0 is the conductance value of the test object before the impact and G_i^1 is the conductance value of the test object

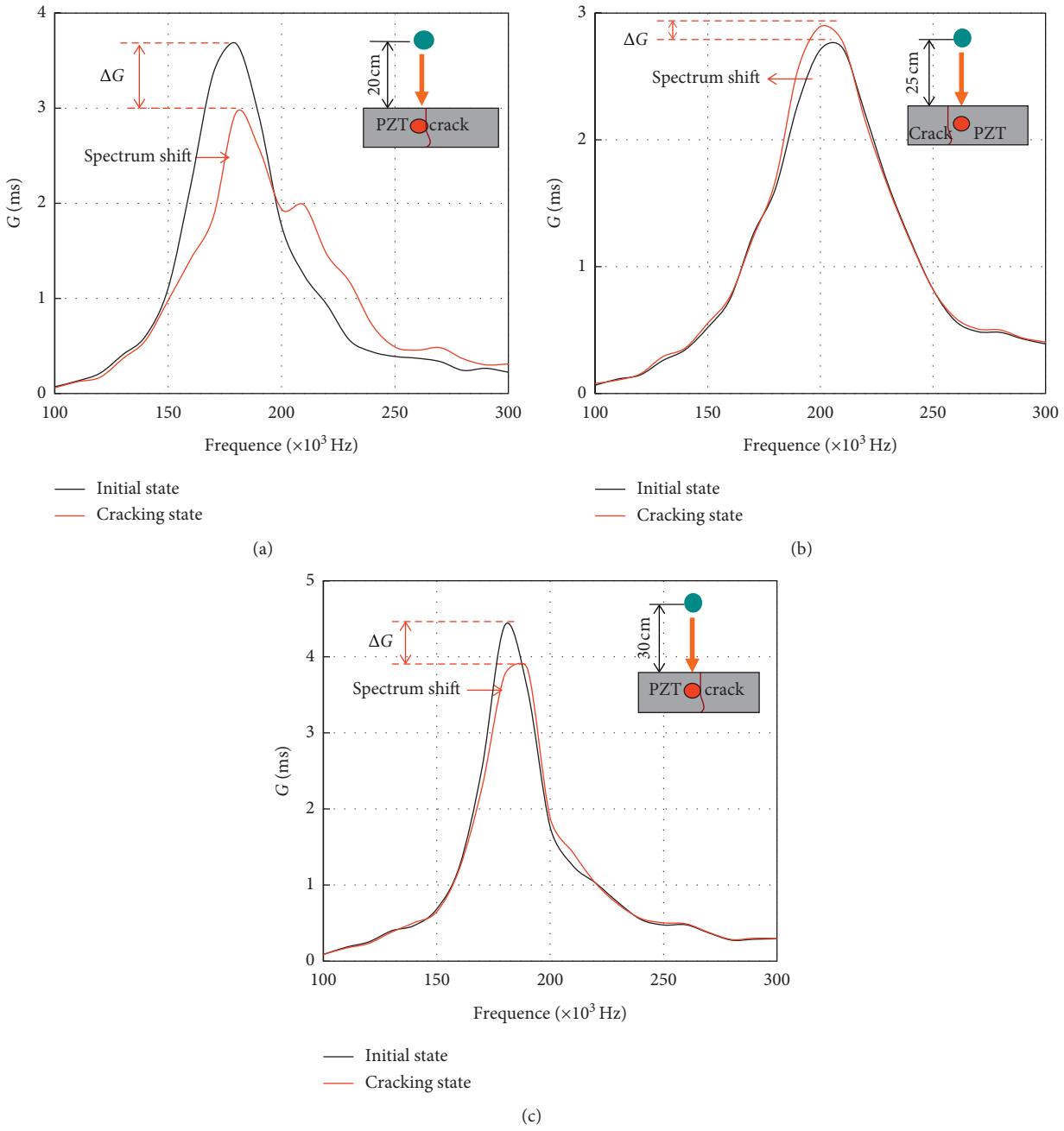

Figure 7: Conductance signal test results in the initial and failure states of the samples: (a) 20 cm; (b) 25 cm; (c) 30 cm.

after the impact ($n \geq 1$). N is the total number of signal sampling points.

The RMSD criterion is adopted in this section to quantitatively analyze the development law of the concrete damage under the impact load. The frequency interval is set as 100–300 kHz, and the number of sampling points is 200. Then, the test results are processed in accordance with equation (1) to obtain the RMSD value of each sample under different impact times, as shown in Figure 8. The analysis reveals the following.

(1) The RMSD value of each sample increases with the impact times, and the overall performance shows changing characteristics of a slow increase in the early stage (Stage I) and a rapid increase in the late stage (Stage II). This pattern shows the typical damage accumulation effect. In the test condition with a low height (20 cm), the slow growth stage in the early stage (damage accumulation process) lasts long.

(2) As indicated by the mechanical mechanism of the concrete damage caused by the low-energy impact load, the internal microcracks of the samples are generated and developed slowly in the early stage. The corresponding output signals of the piezoceramic patch occur gently, whereas the overall damage is gradually accumulated. In the late stage,

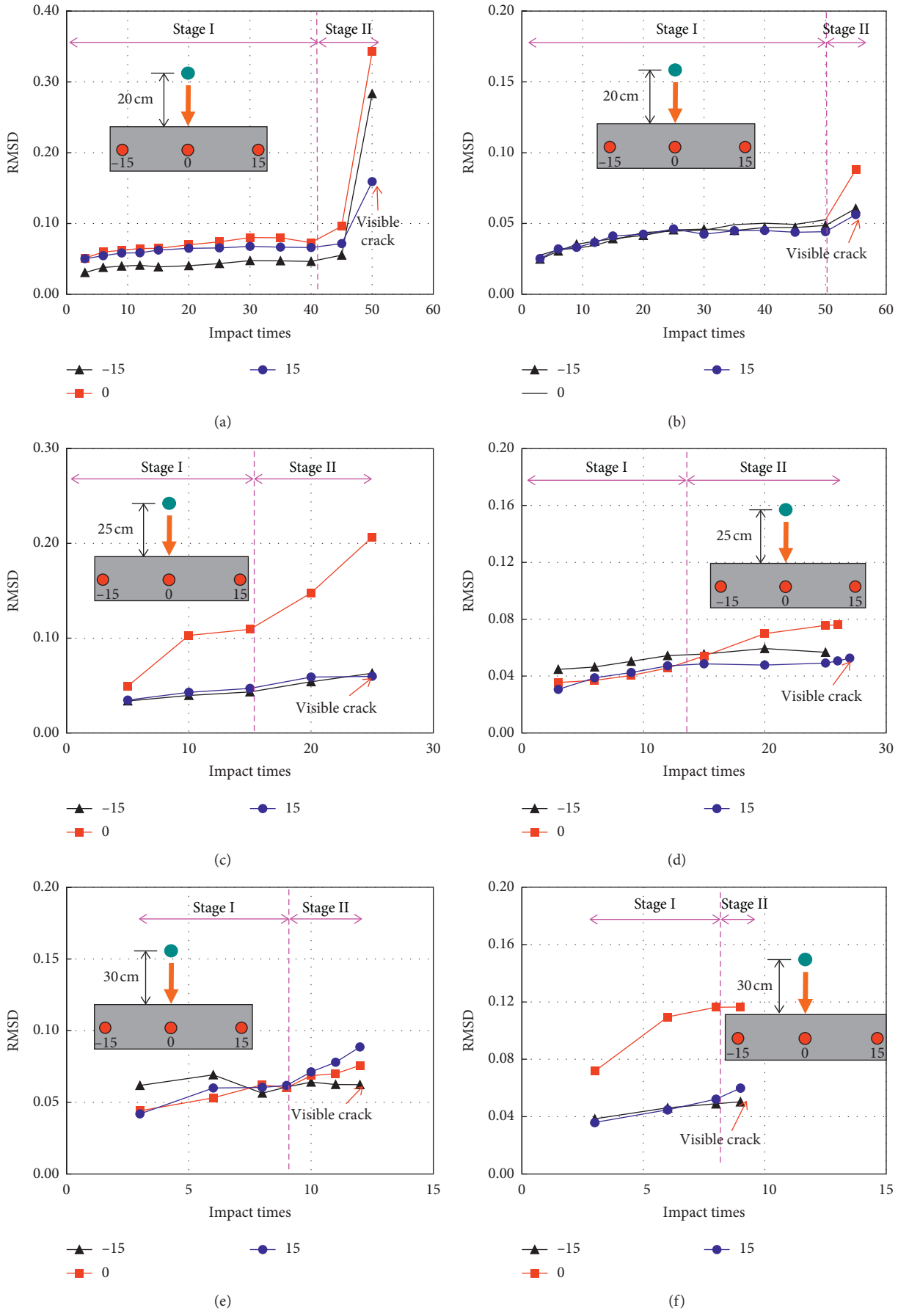

FIGURE 8: Damage evolution curve: (a) 20 cm, sample 1; (b) 20 cm, sample 2; (c) 25 cm, sample 1; (d) 25 cm, sample 2; (e) 30 cm, sample 1; (f) 30 cm, sample 2.

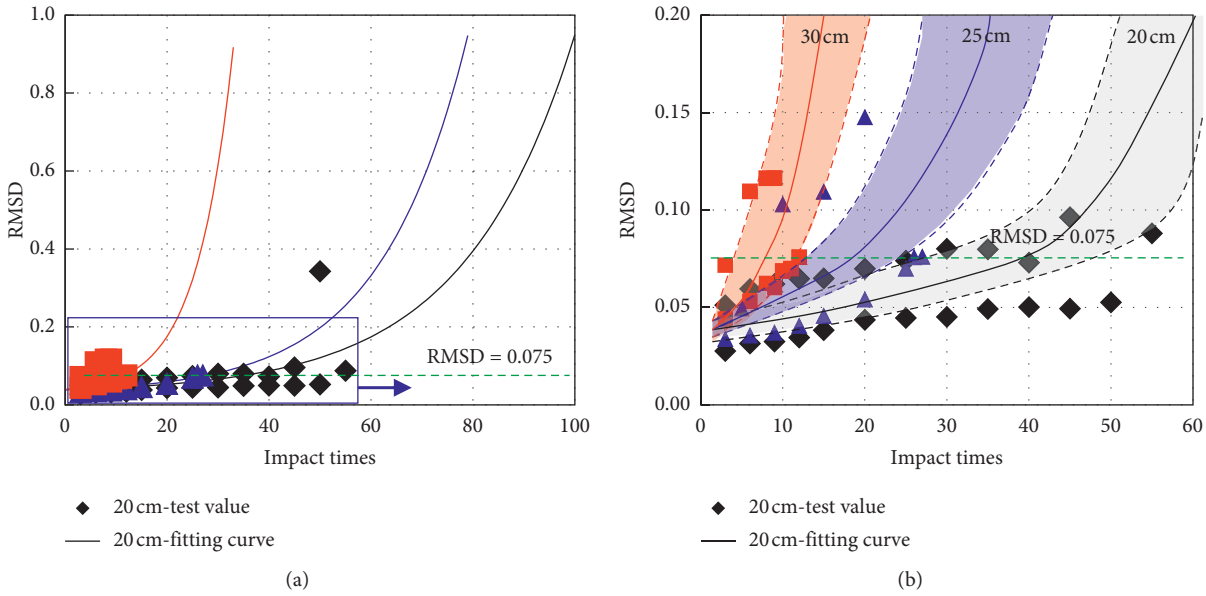

Figure 9: Damage evolution characteristic curves.

under the continuing interaction of the impact load, the internal cracks of the samples continue to develop and connect with each other. Subsequently, the sample damage enters the rapid development stage. Therefore, under the low-energy impact load, the concrete structural damage shows highly nonlinear development. However, under high-energy impact, large crack structures are rapidly formed inside the concrete sample until the cracks connect. Then, the sample quickly forms brittle failure with the noticeable linear growth characteristics of the corresponding piezoceramic patch signal.

(3) The RMSD value at the impact point of the sample changes significantly relative to both ends of the sample. The change in the piezoceramic patch signal is related not only to the damage degree but also to the distance of the paste position to the damaged region. Therefore, the RMSD value at the impact points of each test condition is separately extracted and generalized, obtaining damage evolution characteristic curves shown in Figure 9. The results show that the impact times and RMSD values of the samples follow a typical nonlinear damage evolution trend, which corresponds to the exponential function under impact loads. The one-phase exponential increasing function can well describe the damage evolution:

$$\mathrm{RMSD} = C + Ae^{Bn}, \tag{2}$$

where n is the impact times and A, B, and C are undetermined paraments. Among them, parameter C is mainly influenced by the damage level of stage I,

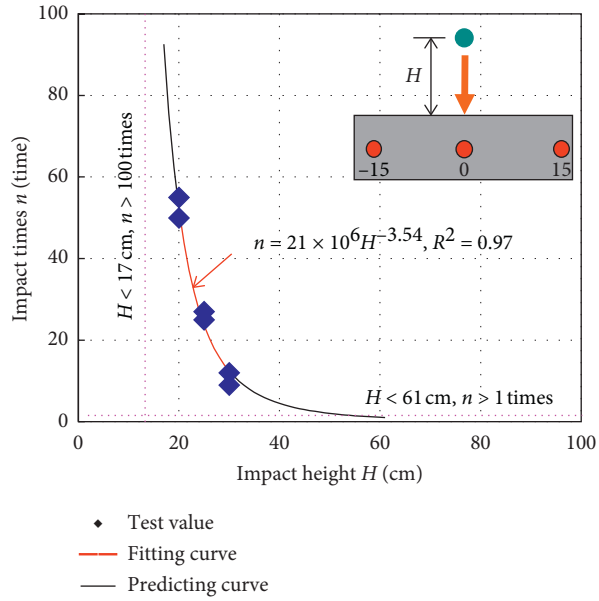

Figure 10: Relationship between the impact height and the limit impact times of the C50 concrete samples.

whereas parameters A and B are decided by the development of RMSD.

The least square fitting method is adopted for parameter determination of each line in Figure 8. According to the fitting results between RMSD and impact times, the differences of parameters C and A are quite limited in the different experimental conditions. However, parameter B has a profound impact on the development of the RMSD and varies obviously under various impact heights. Thus, parameters A and C are calibrated as constant for simplicity according to the

experimental data in Figure 8. Parameter B is further fitted against the impact height to obtain the ideal fitting results. In this experiment, the values of C and A can be determined as $C = 0.03$, $A = 0.009$; the determination of B should further utilize the following function containing the impact height of the heavy ball:

$$B = 0.04 + 1.18 \times 10^{-6} \exp(38H), \quad (3)$$

where H is the height of the impact heavy ball, m.

(4) Further analysis shows that when the RMSD value exceeds 0.075, a rapid growth trend appears with an increase in impact times. This result indicates the entry of the concrete damage into a rapid development stage. Therefore, under the current test conditions, RMSD = 0.075 is regarded as the critical state, where the damage of the sample concrete develops to the critical state, that is, approaching danger or failure. This property can be used to determine the warning state of the concrete structural damage. Moreover, effective reinforced measures are achievable in a timely manner.

(5) The emergence of visible cracks in the sample is a sign of impact failure with the corresponding limit impact times. The relationship curve of the limit impact times of the concrete at different impact heights is shown in Figure 10. Through trial and error, the power function is picked to describe the relation between limited impact times and impact height. The fitting results show power function can better describe the monotone evolution trend between impact times and impact height with high fitting coefficient of 0.98. The corresponding parameters of the power function are calibrated using the experimental data in Figure 10 through least square methods. As shown by the analysis, the limit impact times and impact heights of the samples show the following development law: $n = 2.1 \times 10^6 \cdot H^{-3.54}$. The concrete damage develops slowly when the impact height (energy) is relatively small; under this experiment condition, when the impact height is less than 17 cm, the maximum impact time exceeds 100. The limit impact time decreases sharply (damage life shortens sharply) as the impact height increases. The samples in this experiment can be broken by a single impact when the impact height exceeds 60 cm.

4. Conclusions

A damage evolution characteristic test of C50 nonreinforced concrete under impact loads is conducted by using a self-developed drop-weight impact device and EMI measurement technology. The test results are analyzed, and the following are the main conclusions:

(1) EMI measurement technology has the good identification capacity to the mechanical properties of concrete damage but cannot easily reflect the overall damage state of the samples, whereas the damage evolution of the test objects can be reflected by the RMSD in piezoceramic patch signal better.

(2) The concrete damage is significantly affected by single and cumulative impact energies under the impact load. With low-impact energy, the concrete damage continues to develop for a long time with a remarkable cumulative effect and conspicuous sudden break characteristics will appear before failure. With high-energy impact, the damage accumulates rapidly, and the piezoceramic patch signal grows linearly.

(3) The RMSD of the concrete increases exponentially with the impact times under the impact load. Particularly, when the RMSD value exceeds 0.075, the damage also enters a stage of rapid development, and the concrete approaches the critical failure state. This property can be used to determine the warning state of concrete structural damage and implement effective reinforcement measures in a timely manner.

(4) Under the experiment conditions of this study, the ultimate impact times and heights of the samples show the following trend of the power function. When the impact height (energy) is small, the concrete damage develops slowly. As the impact height (energy) increases, the number of ultimate bearable impact times decreases sharply (damage life shortens drastically).

Data Availability

The data used to support the findings of this study are available from the corresponding author upon request.

Conflicts of Interest

The authors declare that there are no conflicts of interest regarding the publication of this paper.

Acknowledgments

Projects funded by the National Natural Science Foundation of China (Nos. 51978669 and U1934211) and the Natural Science Foundation of Hunan Province, China (No. 2018JJ3657) are gratefully acknowledged. Also, this work was supported by the National Defense Science and Technology Innovation Special Zone.

References

[1] F. P. Sun, Z. Chaudhry, C. Liang, and C. A. Rogers, "Truss structure integrity identification using PZT sensor-actuator," *Journal of Intelligent Material Systems and Structures*, vol. 6, no. 1, pp. 134–139, 1995.

[2] J. W. Ayres III, F. Lalande, C. A. Rogers, and Z. A. Chaudhry, "Qualitative health monitoring of a steel bridge joint via piezoelectric actuator/sensor patches BT," in *Proceedings of the Nondestructive Evaluation of Bridges and Highways*, pp. 211–218, Scottsdale, AZ, USA, December 1996.

[3] J. W. Ayres, F. Lalande, Z. Chaudhry, and C. A. Rogers, "Qualitative impedance-based health monitoring of civil infrastructures," *Smart Materials and Structures*, vol. 7, no. 5, pp. 599–605, 1998.

[4] V. Giurgiutiu, A. Reynolds, and C. A. Rogers, "Experimental investigation of E/M impedance health monitoring for spot-welded structural joints," *Journal of Intelligent Material Systems and Structures*, vol. 10, no. 10, pp. 802–812, 1999.

[5] C. K. Soh, K. K.-H. Tseng, S. Bhalla, and A. Gupta, "Performance of smart piezoceramic patches in health monitoring of a RC bridge," *Smart Materials and Structures*, vol. 9, no. 4, pp. 533–542, 2000.

[6] S. Bhalla, C. K. Soh, K. K. H. Tseng, and A. S. K. Naidu, "Diagnosis of incipient damage in steel structures by means of piezoceramic patches," in *Proceedings of the Eighth East Asia-Pacific Conference*, pp. 5–7, Singapore, December 2001.

[7] K. K. Tseng, "Health monitoring of concrete structures subjected to environmental attacks," *Smart Systems for Bridges, Structures, and Highways*, vol. 4696, pp. 168–175, 2002.

[8] K. K. Tseng and L. Wang, "Smart piezoelectric transducers for in situ health monitoring of concrete," *Smart Materials and Structures*, vol. 13, no. 5, pp. 1017–1024, 2004.

[9] D. Ai, H. Zhu, and H. Luo, "Sensitivity of embedded active PZT sensor for concrete structural impact damage detection," *Construction and Building Materials*, vol. 111, pp. 348–357, 2016.

[10] H. Zhu, H. Luo, D. Ai, and C. Wang, "Mechanical impedance-based technique for steel structural corrosion damage detection," *Measurement*, vol. 88, pp. 353–359, 2016.

[11] N. Liu, L. Peng, C. Shi, and M. Lei, "Experimental and model study on dynamic behaviour and fatigue damage of tunnel invert," *Construction and Building Materials*, vol. 126, pp. 777–784, 2016.

[12] M.-F. Lei, B.-C. Zhou, Y.-X. Lin, F.-D. Chen, C.-H. Shi, and L.-M. Peng, "Model test to investigate reasonable reactive artificial boundary in shaking table test with a rigid container," *Journal of Central South University*, vol. 27, no. 1, pp. 210–220, 2020.

[13] C. Liu, L. Peng, M. Lei, C. Shi, and N. Liu, "Fatigue performance of tunnel invert in newly designed heavy haul railway tunnel," *Applied Sciences*, vol. 9, no. 24, p. 5514, 2019.

[14] C. Liu, M.-F. Lei, L.-M. Peng, and C.-H. Shi, "Cavity influence on fatigue performance of heavy haul railway Tunnel's bottom structure," *Construction and Building Materials*, vol. 251, Article ID 118886, 2020.

[15] C. Liang, F. Sun, and C. A. Rogers, "Electro-mechanical impedance modeling of active material systems," *Smart Materials and Structures*, vol. 5, no. 2, pp. 171–186, 1996.

[16] C. Liang, F. P. Sun, and C. A. Rogers, "An impedance method for dynamic analysis of active material systems," *Journal of Vibration and Acoustics*, vol. 116, no. 1, pp. 120–128, 1994.

[17] S. Park, S. Ahmad, C.-B. Yun, and Y. Roh, "Multiple crack detection of concrete structures using impedance-based structural health monitoring techniques," *Experimental Mechanics*, vol. 46, no. 5, pp. 609–618, 2006.